Methodology for Sensorless Displacement Control on a Homopolar Bearingless Motor

Zeqiang HE*, Tadahiko SHINSHI **
*Department of Mechanical Engineering, Institute of Science Tokyo
Yokohama, Kanagawa 226-8501, Japan
**Institute of Innovative Research, Institute of Science Tokyo
Yokohama, Kanagawa 226-8501, Japan
E-mail: shinshi.t.ab@m.titech.ac.jp

Abstract
Bearingless slice motors (BELMs) integrate a motor and a radial magnetic bearing within a shared stator core, allowing for rotor tilt and axial stabilization through passive magnetic coupling. However, incorporating mechanical sensors for both rotation and displacement control within a limited space increases system complexity and cost. To address this, we propose a robust sensorless displacement control method for BELMs with separated windings. The approach utilizes the voltage difference between centrally symmetrical armature coils, where coil terminal voltage (CTV) contains high-SNR radial displacement information, unlike the low-SNR phase terminal voltage (PTV). High-frequency signals are injected to enhance SNR and enable accurate, fast displacement estimation without interfering with suspension current control.

Keywords : Bearingless motor, Sensorless control, Magnetic suspension, Coil terminal voltage

1. Introduction

The Bearingless Slice Motor (BELM) is gaining attention in fields like semiconductor manufacturing and ultra-pure pumping due to its contactless operation and seal-free structure (Chen et al., 2020). However, its adoption is limited by the high cost and environmental sensitivity of rotor displacement sensors. This has led to growing interest in sensorless displacement control.

Initially developed in active magnetic bearings (AMBs), sensorless techniques—particularly high-frequency signal injection (HFSI)—estimate rotor position by analyzing induced electromotive force (EMF) from high-frequency voltages applied to stator windings. While effective in cylindrical rotor AMBs, HFSI struggles in BELMs with solid-core rotors due to eddy current attenuation and in systems with combined windings due to frequency interference between the armature and suspension circuits. These challenges lower the signal-to-noise ratio (SNR) and hinder the reliable estimation of displacement.

Recent studies, such as those by Chen and Zhou (2021), Lei et al. (2024), and Cui et al. (2024), have attempted to apply HFSI to various types of BELM. They have been limited by frequency overlaps and integrated winding interference. Furthermore, the proposed methods depend on angular sensors, which are bulky and costly, making high-SNR, sensorless displacement control without angle feedback a continuing challenge in BELM research. Although BELMs with separated windings offer a potential solution by decoupling torque and levitation functions, existing HFSI methods remain ineffective due to the lack of position-dependent signals in the phase-terminal voltages (PTVs).

This study presents a novel sensorless method for estimating radial displacement in BELMs with separated windings, eliminating the need for rotor angle sensors. The approach utilizes high signal-to-noise ratio (SNR) differences in coil-terminal voltages (CTV) between symmetrical armature coils, which provide position-dependent information. To enhance this signal, a high-frequency voltage is injected into the armature coils. Due to the magnetic decoupling of the suspension windings, the suspension current remains unaffected, allowing for clean control. The method has been experimentally validated on a homopolar bearingless reluctance slice motor (HBSRM) with a bulk iron rotor, confirming its effectiveness even under nonlinear magnetic conditions.

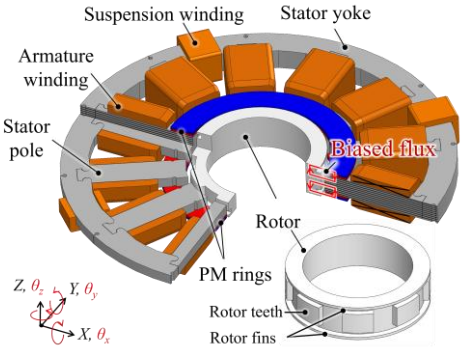

Fig. 1 Structure of the HBSRM.

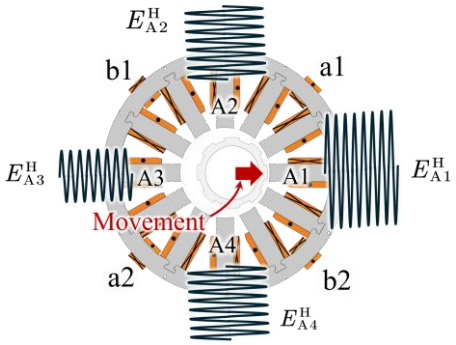

Fig. 2 Illustration of the sensorless displacement estimation using high-frequency EMF of CTVs.

2. HBSRM structure and sensorless method

2.1 HBSRM

To illustrate the methodology based on the CTV concept, we employ the sensorless displacement method to an HBSRM shown in Fig. 1. The HBSRM consists of a stator core, armature winding, suspension winding, permanent magnet (PM) rings, and a reluctance rotor. The stator core is made from laminated silicon steel, while the rotor is made of soft, bulky iron, which allows for complex machining of salient structures on its surface. The stator and rotor are designed with a 12/8 pole configuration, and the rotor poles feature a two-dimensional salient array in both the axial and circumferential directions, as shown in the enlarged view. Two axially magnetized PM sliced rings are mounted on the top and bottom of the stator pole tips to induce a circularly biased homopolar flux in the air gap. It should be noted that all the PM biased flux flows towards the rotor in the plane, forming a homopolar field in the air gap.

The HBSRM adopts a separate winding configuration, with three-phase armature windings on the stator poles and two-phase suspension windings on the stator yoke, as shown in Fig. 2. The armature winding current induces torque on the rotor, while the suspension current regulates the radial force on the rotor. The suspension windings consist of four coils, with *a1* and *a2* coils for phase *a* and *b1* and *b2* coils for phase *b*. The coils of the same suspension winding phase are connected in series. On the other hand, each phase of armature winding consists of four coils, with the centrally symmetrical coils connected in series to form one branch of each phase. Specifically, *A1* and *A3* coils are connected in series, in parallel with the branch formed by serially connected *A2* and *A4* coils. Two H bridges and one three-phase half-bridge inverter are employed to drive the armature and suspension windings independently.

2.2 CTV

To estimate the radial position of the rotor, it is necessary to select an appropriate CTV signal. To mitigate frequency overlap, the armature windings are chosen over the suspension windings, as the control voltage in the latter typically exhibits a broad frequency spectrum, resulting in substantial signal interference. In the A-phase armature winding, four coils are distributed symmetrically, two aligned along the X-axis and two along the Y-axis. For improved signal integrity, the coils aligned along the same axis are connected in series and are hereafter denoted as coils *A1*, *A2*, *A3*, and *A4* in sequential order.

2.3 High frequency signal injection

To enable the displacement estimation at zero speed, we propose injecting an HF voltage into the stationary α axis of the three-phase armature winding. This HF excitation amplifies the voltage differential between symmetrically placed armature coils, thereby enhancing the observability of rotor displacement. The injected HF voltage takes the form $U_{\alpha}^{\mathrm{H}}\cos(\omega_{\mathrm{H}}t)$, where U_{α}^{H} is the amplitude of the voltage and ω_{H} is the injected frequency. Both parameters significantly influence the quality of the resulting voltage differential. In particular, ω_{H} must be made carefully to avoid frequency overlap with the control voltage associated with the armature current. The frequency content of the control voltage in the armature winding becomes negligible beyond 1 kHz, thereby facilitating the extraction of a low-noise HF signal from the CTVs.

The principle based on the HFSI and CTV can be briefly explained in Fig. 2. When the rotor moves towards the *A1* coil, the HF voltage in the *A1* coil will be more significant than that of the *A3* coil due to the asymmetrical reluctance. On the contrary, the HF voltage in the *A3* coil will be amplified if the rotor moves towards *A3* coil. This asymmetrical voltage response serves as a reliable indicator of rotor displacement, enabling accurate position estimation even at zero or low rotational speeds.

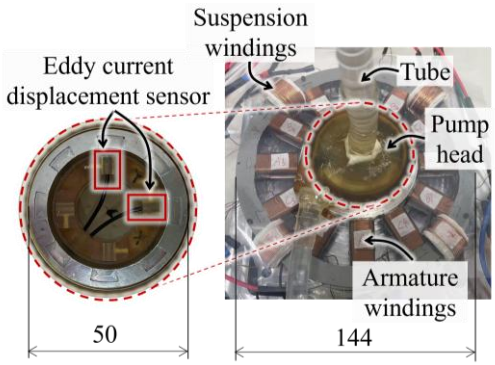

Fig. 3 Experiment setup of the sensorless displacement control.

2.4 Estimation method

Provided that CTVs in four A-phase armature coils are measured to be E_{A1}, E_{A2}, E_{A3} and E_{A4}, we can extract the HF components as $E_{\mathrm{A1}}^{\mathrm{H}}$, $E_{\mathrm{A2}}^{\mathrm{H}}$, $E_{\mathrm{A3}}^{\mathrm{H}}$ and $E_{\mathrm{A4}}^{\mathrm{H}}$ via a bandpass filter. It should be noted that the sum of $E_{\mathrm{A1}}^{\mathrm{H}}$ and $E_{\mathrm{A3}}^{\mathrm{H}}$ is exactly the injected HF voltage $U_{\alpha}^{\mathrm{H}}\cos(\omega_{\mathrm{H}}t)$. Meanwhile, the difference between $E_{\mathrm{A1}}^{\mathrm{H}}$ and $E_{\mathrm{A3}}^{\mathrm{H}}$, i.e., $E_{\mathrm{A1}}^{\mathrm{H}}-E_{\mathrm{A3}}^{\mathrm{H}}$, is proportional to the product of rotor displacement in the X axis and the injected HF voltage:

$$E_{\mathrm{A1}}^{\mathrm{H}}-E_{\mathrm{A3}}^{\mathrm{H}} \propto x\, U_{\alpha}^{\mathrm{H}}\cos(\omega_{\mathrm{H}}t) \tag{1}$$

We propose to modulate the voltage difference, yielding

$$U_M \triangleq U_{\alpha}^{\mathrm{H}}\cos(\omega_{\mathrm{H}}t)\,(E_{\mathrm{A1}}^{\mathrm{H}}-E_{\mathrm{A3}}^{\mathrm{H}}) \propto \frac{x}{2}(U_{\alpha}^{\mathrm{H}})^2[1+\cos(2\omega_{\mathrm{H}}t)] \tag{2}$$

The modulated signal U_M contains the DC rotor radial displacement, while perturbed by the high-frequency component $\cos(2\omega_{\mathrm{H}}t)$. Considering that the perturbation features a much higher frequency than the mechanical motion of the rotor, it is reasonable to employ a low-pass filter (LPF) of 150 Hz to suppress the alternating perturbation from the DC component. Consequently, the radial displacement of the rotor in the X and Y directions can be estimated to be

$$\begin{cases} \hat{x}=\eta\cdot LPF[(E_{\mathrm{A1}}^{\mathrm{H}}+E_{\mathrm{A3}}^{\mathrm{H}})(E_{\mathrm{A1}}^{\mathrm{H}}-E_{\mathrm{A3}}^{\mathrm{H}})] \\ \hat{y}=\eta\cdot LPF[(E_{\mathrm{A2}}^{\mathrm{H}}+E_{\mathrm{A4}}^{\mathrm{H}})(E_{\mathrm{A2}}^{\mathrm{H}}-E_{\mathrm{A4}}^{\mathrm{H}})] \end{cases} \tag{3}$$

where the coefficient η is the ratio that can be fitted ahead.

3. Experiment setup and result

3.1 Experiment setup

We fabricated a prototype of the HBSRM and tested the proposed sensorless displacement control method on the prototype to verify the methodology. As the HBSRM is targeted at the blood pump, we built the prototype with the pump housing. Additionally, the rotor in the figure is machined from solid-core iron and coated with a polycarbonate material. To simulate extracorporeal circulation, we machine the blade on the rotor top and fill the pump head with a 40 wt% glycerol solution to simulate blood viscosity. Fig. 3 shows the hardware configuration of the system. We place two eddy current displacement sensors inside the rotor to measure the reference radial displacement for accuracy evaluation. The armature and suspension windings are driven by three-phase insulated gate bipolar transistor inverters (STEVAL-IPM07F, STMicro, Europe) using pulse width modulation.

3.2 Experiment result

Fig. 4 illustrates the sensorless displacement control during both startup and stable suspension. It takes approximately 0.15 seconds for the rotor to center from the touchdown wall. The rotor exhibits a radial vibration of approximately ±0.08 mm, with a maximum estimation error of 0.045 mm. Notably, this vibration mainly arises from the significant phase delay introduced by the eddy current effect of the iron rotor.

A frequency response analysis (FRA) experiment is conducted to evaluate the phase delay at different frequencies. We actively offset the radial displacement reference to be a sinusoid function with an amplitude of 0.02 mm, and swept the frequency from 0.1 Hz to 100 Hz. The FRA result is shown in Fig. 5. While the bandwidth of the magnitude where the attenuation is -3 dB reaches 56 Hz, the bandwidth of the phase at -90 degrees is approximately 16Hz, leading to

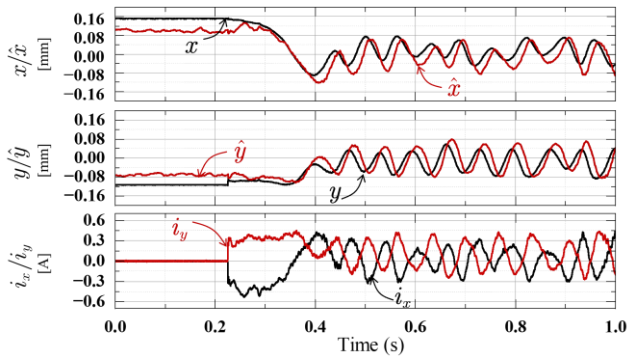

Fig. 4 Experiment result of radial displacement response during the sensorless control suspension startup.

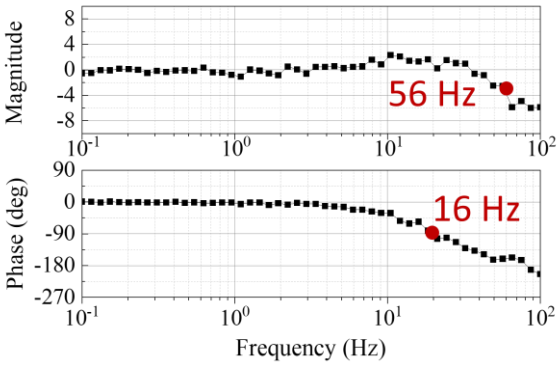

Fig. 5 Experiment result of FRA of $\hat{x}/x$ from 0.1 Hz to 100 Hz

severe radial vibration. The phenomenon reveals the fact that the eddy current effect on the iron rotor introduces a significant undesired phase delay, even at 16 Hz, causing an estimation error in the proposed method.

4. Conclusion and future work

This paper ingeniously solves the frequency overlap problem in the sensorless suspension control of the BELM by proposing the concept of CTV. Based on CTV concept, we designed and fabricated HBSRM and managed to achieve sensorless suspension control in the pump setting. However, due to the severe eddy current effect of the solid-core rotor, a significant phase delay occurs in the displacement estimate, resulting in noticeable radial vibration. In the future, we would like to reduce the phase delay by replacing the solid-core rotor with a material that resists the eddy current effect.

References

Chen, J., Zhu, J. and Severson, E. L., Review of bearingless motor technology for significant power applications, IEEE Transactions on Industry Applications, Vol. 56, No. 2 (2020), pp. 1377–1388.

Chen, Y. and Zhou, Y., Radial displacement sensorless control of bearingless flux-switching permanent magnet machines based on difference of symmetric-winding flux linkages, IEEE Transactions on Industrial Electronics, Vol. 68, No. 9 (2021), pp. 7793–7803.

Lei, Z., Wu, X., Wu, T., Yu, X., Mi, Y. and Huang, S., Radial displacement sensorless control at low speed based on high-frequency voltage injection for bearingless permanent magnet vernier motor with special winding, IEEE Transactions on Transportation Electrification, Vol. 11, No. 3 (2025), pp. 7171-7183.

Cui, Z., Zhou, Y. and Zhou, Y., Research on rotor radial position observation method of dual-winding bearingless flux-switching permanent magnet machines, IEEE Transactions on Industrial Electronics, Vol. 71, No. 7 (2024), pp. 6622–6634.

Yang, R., He, Z., Sugita, N. and Shinshi, T., Low-cost and compact disposable extracorporeal centrifugal blood pump utilizing a homopolar bearingless switched reluctance slice motor, IEEE Access, Vol. 11 (2023), pp. 24353-24366.

He, Z., Sugita, N. and Shinshi, T., A novel heteropolar bearingless slice motor with a PM-free rotor for centrifugal blood pump applications, IEEE Access, Vol. 11 (2023), pp. 100114–100124.